EVS29 Symposium
Montréal, Québec, Canada, June 19 - 22, 2016

Fundamental Research on Range Extension Autonomous Driving for Electric Vehicle Based on Optimization of Vehicle Velocity Profile in Consideration of Cornering

Yuta Ikezawa[1], Hiroshi Fujimoto
Daisuke Kawano[2], Yuichi Goto
Misaki Tsuchimoto[3], Koji Sato
[1]*The University of Tokyo, 5-1-5, Kashiwanoha, Kashiwa, Chiba, 277-8561, Japan, ikezawa14@hflab.k.u-tokyo.ac.jp*
[2]*National Traffic Safety and Environment Laboratory, 7-42-27, Jindaijihigashimachi, Chofu, Tokyo, 182-0012, Japan*
[3]*Ono Sokki Co.,Ltd., 3-9-3, Shin-Yokohama, Kohoku-ku, Yokohama, Kanagawa, 222-8507, Japan*

Abstract

Electric vehicles (EVs) have been intensively studied over the past decade, owing to their environmentally-friendly characteristics, however, their miles-per-charge is relatively short. To improve the miles-per-charge, the authors' group has proposed Range Extension Autonomous Driving (READ) system which minimizes the consumption energy by optimizing the velocity profile. This paper extends READ system to be applied to not only straight driving but also curvy road by modeling the vehicle rotation motion and the cornering resistance. The effectiveness of the proposed method is verified by simulations and experiments.

Keywords: EV (electric vehicle), optimization, energy consumption, range

1 Introduction

Due to the increasing concerns on environmental and energy problems, many kinds of research have been conducted in the last decade. As one of the countermeasures for this problem, the electric vehicles (EVs) have attracted great attention due to its environmentally-friendly characteristics. Compared with internal combustion engine vehicles (ICEVs), EVs have the following remarkable advantages [1].

1. Torque generation of a motor is faster than that of an engine (several milliseconds vs. several hundred milliseconds).
2. Motor torque can be estimated precisely from the current.
3. For EVs with in-wheel motors, each wheel can be controlled independently.
4. Motors not only can be used for driving, but also can be employed for regenerative braking.

However, the miles-per-charge of typical EVs is shorter than the cruising range of typical ICEVs. To improve the miles-per-charge, many kinds of research have been conducted, for example, designing high efficiency motors [2], series chopper power train using a buck-boost chopper [3], and wireless power transfer for moving EVs [4].

On the other hand, some research solve the energy problem by improving traffic flow by using Intelligent Transport Systems (ITS) [5]. Traffic flow is improved by platooning running using the information of the front and rear vehicles [6], and by introducing virtual traffic lights [7]. Along with the development of ITS and autonomous driving technologies, the vehicle velocity can be designed by considering objectives such as energy efficiency, i.e., energy consumption can be reduced by optimizing the velocity profile. The authors' research group has proposed the Range Extension Autonomous Driving (READ) system, which improves the miles-per-charge by optimizing the velocity profile numerically on the assumption that the stop point and gradient information are acquired from ITS [8, 9].
However, conventional READ system can be applied to only straight driving. In this paper, the READ system is extended to be applied to not only straight driving but also curvy road by modeling vehicle rotating motion and the cornering resistance. The effectiveness of the proposed method is verified by simulations and experiments.

2 Vehicle Model

In this section, vehicle motion and inverter input power are modeled. Inverter input power model is needed to modify the control input when optimizing the velocity profile numerically.

2.1 Experimental Vehicle

In this research, an original electric vehicle "FPEV-2 Kanon," manufactured by the authors' research group, is used. Fig. 1 and Table 1 show the experimental vehicle and its specifications, respectively. This vehicle has four outer-rotor type in-wheel motors which can be independently controlled. Therefore, driving-braking force distribution among the four wheels is possible. Table 2 shows the specifications of the in-wheel motors. Efficiency maps of the front and rear in-wheel motors are different as shown in Fig. 2.

Figure 1: FPEV2-Kanon.

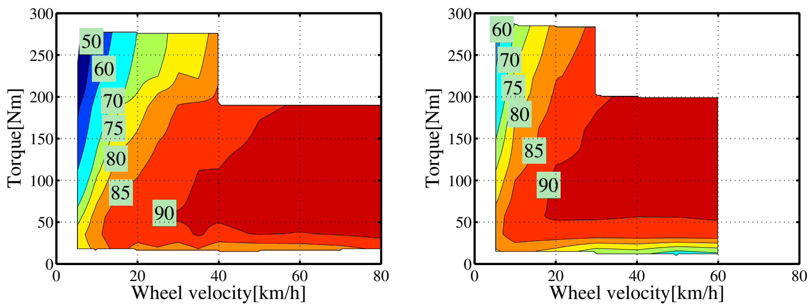

(a) Front motor.

(b) Rear motor.

Figure 2: Efficiency maps of front and rear motors.

Table 1: Vehicle specification.

Vehicle mass M	854 kg
Wheelbase l	1.72 m
Distance from center gravity to front and rear axle l_f,l_r	l_f:1.01 m l_r:0.702 m
Height of gravitational center h_g	0.510 m
Front wheel inertia J_{ω_f}	1.24 kg·m^2
Rear wheel inertia J_{ω_r}	1.26 kg·m^2
Wheel radius r	0.302 m
Front cornering stiffness C_f	12.5 kN/rad
Rear cornering stiffness C_r	28.2 kN/rad

Table 2: Specification of in-wheel motors.

	Front	Rear
Manufacturer	TOYO DENKI SEIZO K.K.	
Type	Direct Drive System	
Rated torque	110 Nm	127 Nm
Maximum torque	500 Nm	530 Nm
Rated power	6.00 kW	6.00 kW
Maximum power	20.0 kW	25.0 kW
Rated speed	382 rpm	450 rpm
Maximum speed	1110 rpm	1200 rpm

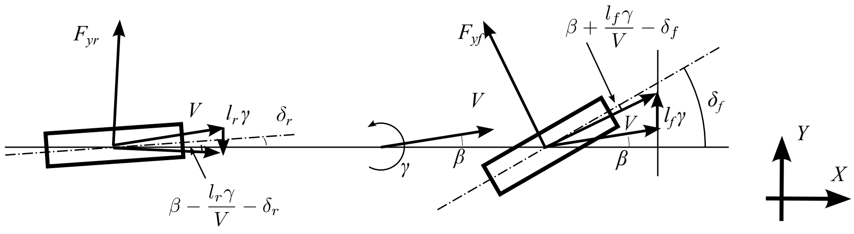

Figure 3: Bicycle model of vehicle dynamics.

2.2 Vehicle Model

In this section, a four wheel driven vehicle is modeled.

2.2.1 Equation of Vehicle Dynamics

In this paper, bicycle model shown in Fig. 3 is considered, and the torques of the right and left motors are equal. The equations of the wheel rotation and the vehicle dynamics are given as

$$J_{\omega_j}\dot{\omega}_j = T_j - rF_j, \quad (1)$$

$$M\dot{V} = F_{\text{all}} - \text{sgn}(V)(F_{\text{DR}} + F_{\text{CR}}), \quad (2)$$

$$Ma_y = MV(\dot{\beta} + \gamma) = -2Y_f - 2Y_r, \quad (3)$$

$$I\dot{\gamma} = 2(-l_fY_f + l_rY_r), \quad (4)$$

where J_{ω_j} is the wheel inertia, ω_j is the wheel angular velocity, T_j is the motor torque, r is the wheel radius, F_j is the driving-braking force of each wheel, M is the vehicle mass, V is the vehicle velocity, F_{all} is the total driving-braking force, sgn is a sign function, F_{DR} is the driving resistance, F_{CR} is the cornering resistance, a_y is the lateral acceleration, β is the side slip angle of the vehicle, γ is the yaw rate, Y_j is the lateral force of each tyre, I is the inertia around z-axis, and l_j is the distance from the center of gravity to front and rear axle. The subscript j represents f or r (f stands for front and r represents rear). The total driving force is distributed equally among four wheels.

$$F_f = F_r = \frac{1}{4}F_{\text{all}}. \quad (5)$$

The driving resistance F_{DR} is defined as

$$F_{\text{DR}}(V) = \mu_0 Mg + b|V| + \frac{1}{2}\rho C_d AV^2, \quad (6)$$

where μ_0 is the rolling friction coefficient, b is a factor proportional to V, ρ is the air density, C_{d} is the drag coefficient, and A is the frontal projected area.

2.2.2 Lateral Force and Cornering Resistance

The lateral force and the cornering resistance applying to the front tyre is shown in Fig. 4. The cornering force F_{yj} is described as

$$F_{yj} = -C_j\alpha_j, \quad (7)$$

where C_j is the cornering stiffness, α_j is the tyre slip angle.
If the tyre slip angle is small enough, the cornering force is supposed to be roughly equal to the tyre lateral force Y_j.

$$Y_j \simeq F_{yj} = -C_j\alpha_j. \quad (8)$$

Define $F_{\text{CR}}{}'$ as the traveling direction component force of the tyre lateral force, $F_{\text{CR}}{}'$ is given as

$$F_{\text{CR}}{}' \simeq -2Y_f\sin\alpha_f - 2Y_r\sin\alpha_r \simeq 2C_f{\alpha_f}^2 + 2C_r{\alpha_r}^2. \quad (9)$$

Define $F_{\rm CR}$ as the x-direction component force of $F_{\rm CR}'$, $F_{\rm CR}$ is given as

$$F_{\rm CR} \simeq 2C_f{\alpha_f}^2\cos\delta_f + 2C_r{\alpha_r}^2\cos\delta_r \simeq 2C_f{\alpha_f}^2 + 2C_r{\alpha_r}^2. \tag{10}$$

The tyre slip angle α_f, α_r are described as

$$\alpha_f(V,\beta,\gamma,\delta_f) = \beta + \frac{l_f\gamma}{V} - \delta_f, \tag{11}$$

$$\alpha_r(V,\beta,\gamma) = \beta - \frac{l_r\gamma}{V}, \tag{12}$$

where δ_f is the front steering angle.

Assuming that the vehicle is brought into stationary circular turn ($\dot\beta = 0$, $\dot\gamma = 0$), the side slip angle of the vehicle, the yaw rate, the front steering angle, and the tyre slip angle are expressed as a function of the velocity and the turning radius R.

$$\beta(V,R) \simeq (1-BV^2)\frac{l}{R}, \tag{13}$$

$$\gamma(V,R) \simeq \frac{V}{R}, \tag{14}$$

$$\delta_f(V,R) \simeq (1+AV^2)\frac{l}{R}, \tag{15}$$

$$\alpha_f(V,R) \simeq -AV^2\frac{l}{R} - BV^2\frac{l_r}{R}, \tag{16}$$

$$\alpha_r(V,R) \simeq -BV^2\frac{l_r}{R}, \tag{17}$$

where A and B are respectively constant given by

$$A = -\frac{M}{2l^2}\frac{l_fC_f - l_rC_r}{C_fC_r}, \tag{18}$$

$$B = \frac{M}{2l}\frac{l_f}{l_rC_r}. \tag{19}$$

Therefore cornering resistance is expressed as a function of the velocity and the turning radius.

$$F_{\rm CR}(V,R) \simeq \frac{M^2}{2l^2}\left(\frac{{l_r}^2}{C_f} + \frac{{l_f}^2}{C_r}\right)\frac{V^4}{R^2}. \tag{20}$$

2.2.3 Slip ratio

The slip ratio λ_j is given as

$$\lambda_j = \frac{V_{\omega_j} - V}{\max(V_{\omega_j}, V, \epsilon)}, \tag{21}$$

where $V_{\omega_j} = r\omega_j$ is the wheel speed and ϵ is a small constant to avoid division by zero. It is known that the slip ratio λ is related with the friction coefficient μ as shown in Fig. 5 [10]. In the region of $|\lambda| \ll 1$, μ is nearly proportional to λ. Define the driving stiffness $D_{\rm s}'$ as the slope of the curve, the driving-braking force of each wheel is given as

$$F_j = \mu_jN_j \simeq {D_s}'N_j\lambda_j, \tag{22}$$

where N_j is the normal force of each wheel. When driving at V and $F_{\rm all}$, N_f and N_r are respectively calculated as

$$N_f(V,F_{\rm all},R) = \frac{1}{2}\left[\frac{l_r}{l}Mg - \frac{h_{\rm g}}{l}\{F_{\rm all} - {\rm sgn}(V)(F_{\rm DR}(V) + F_{\rm CR}(V,R))\}\right], \tag{23}$$

$$N_r(V,F_{\rm all},R) = \frac{1}{2}\left[\frac{l_f}{l}Mg + \frac{h_{\rm g}}{l}\{F_{\rm all} - {\rm sgn}(V)(F_{\rm DR}(V) + F_{\rm CR}(V,R))\}\right], \tag{24}$$

where l is the wheelbase and $h_{\rm g}$ is the height of gravitational center. In this paper, lateral load variation during cornering is neglected.

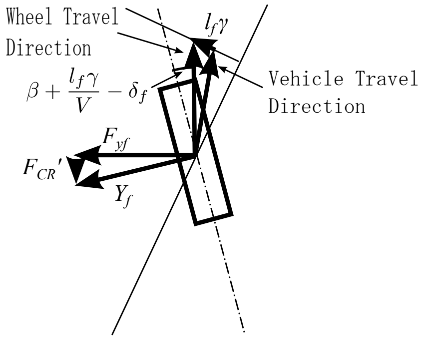

Figure 4: Cornering resistance of front tyre.

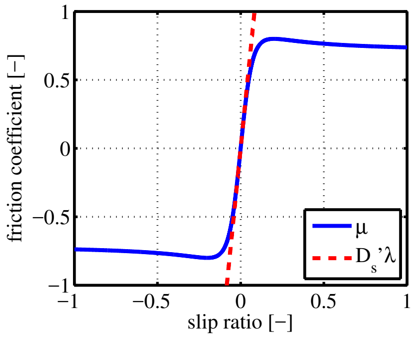

Figure 5: μ-λ Curve [10].

2.3 Inverter Input Power Model

In this subsection, the inverter input power is modeled. Neglecting the mechanical loss of the motor and the inverter loss, the inverter input power P_{in} is described as

$$P_{\text{in}} = P_{\text{out}} + P_{\text{c}} + P_{\text{i}}, \tag{25}$$

where P_{out} is the sum of the mechanical outputs of each motor, P_{c} is the sum of the copper losses of each motor, and P_{i} is the sum of the iron losses of each motor [11]. In this paper, wheel speed difference between left and right is neglected during cornering.
Suppose that the torque caused by the wheel inertia and slip ratio λ_j are small enough. Then the motor torque T_j and the wheel angular velocity ω_j are given as

$$T_j \simeq rF_j, \tag{26}$$

$$\omega_j \simeq \frac{V}{r}(1+\lambda_j). \tag{27}$$

Therefore P_{out} is calculated as

$$P_{\text{out}} = 2\sum_{j=f,r} \omega_j T_j \simeq \frac{VF_{\text{all}}}{2} \sum_{j=f,r} \left(1 + \frac{F_{\text{all}}}{4D_s{}'N_j(V, F_{\text{all}})}\right). \tag{28}$$

In the modeling of the copper loss P_{c}, the iron loss resistance is neglected for simplicity. Suppose that the magnet torque and the q-axis current are much larger than the reluctance torque and the d-axis current, respectively. Then, the sum of the copper losses P_{c} is given as

$$P_{\text{c}} = 2\sum_{j=f,r} R_j {i_{qj}}^2 \simeq \frac{r^2}{8} {F_{\text{all}}}^2 \sum_{j=f,r} \frac{R_j}{{K_{\text{t}j}}^2}, \tag{29}$$

where R_j is the armature winding resistance of the motor, i_{qj} is the q-axis current, and $K_{\text{t}j}$ is the torque coefficient of the motor.
Next, the iron loss is modeled. In this paper, based on the well-known equivalent circuit model [12]. Fig. 6 shows the d and q-axis equivalent circuits of the permanent magnetic synchronous motor. From Fig. 6, the sum of the iron losses P_{i} is expressed as

$$\begin{aligned} P_{\text{i}} &= 2\sum_{j=f,r} \frac{{v_{odj}}^2 + {v_{oqj}}^2}{R_{\text{c}j}} = 2\sum_{j=f,r} \frac{{\omega_{\text{e}j}}^2}{R_{\text{c}j}} \left\{ (L_{dj} i_{odj} + \Psi_j)^2 + (L_{qj} i_{oqj})^2 \right\} \\ &\simeq 2\frac{V^2}{r^2} \sum_{j=f,r} \frac{{P_{\text{n}j}}^2}{R_{\text{c}j}} \left\{ \left(\frac{rL_{qj}F_{\text{all}}}{4K_{\text{t}j}} \right)^2 + {\Psi_j}^2 \right\} \end{aligned} \tag{30}$$

where v_{odj} and v_{oqj} are respectively the d and q-axis induced voltages, $R_{\text{c}j}$ is the equivalent iron loss resistance, $\omega_{\text{e}j}$ is the electrical angular velocity of each motor, L_{dj} is the d-axis inductance, L_{qj} is the

q-axis inductance, i_{odj} and i_{oqj} are respectively the differences between the d and q-axis currents and the d and q-axis components of the iron loss current, $P_{\mathrm{n}j}$ is the number of pole pairs, and Ψ_j is the interlinkage magnetic flux. The equivalent iron loss resistance $R_{\mathrm{c}j}$ is described as

$$\frac{1}{R_{\mathrm{c}j}(\omega_{\mathrm{e}j})} = \frac{1}{R_{\mathrm{c}0j}} + \frac{1}{R_{\mathrm{c}1j}{}'|\omega_{\mathrm{e}j}|}. \tag{31}$$

In (31), the first and second terms of right hand side are the eddy current loss and the hysteresis loss, respectively.
Therefore inverter input power P_{in} can be expressed as a function of the velocity V and the total driving force F_{all}.

$$P_{\mathrm{in}}(V, F_{\mathrm{all}}) = P_{\mathrm{out}}(V, F_{\mathrm{all}}) + P_{\mathrm{c}}(F_{\mathrm{all}}) + P_{\mathrm{i}}(V, F_{\mathrm{all}}). \tag{32}$$

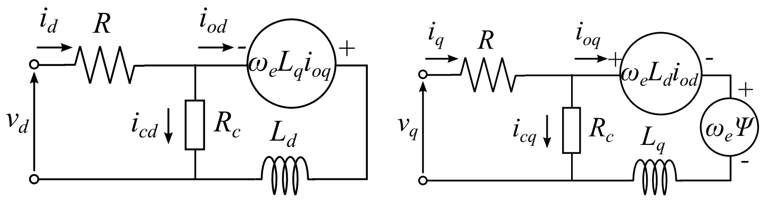

(a) d-axis. (b) q-axis.

Figure 6: Equivalent circuit of PMSM [12].

3 Range Extension Autonomous Driving

In this paper, the vehicle velocity is assumed to be changed from V_0 to V_{f} with a fixed travel distance $X_{\mathrm{f}} - X_0$ and a fixed traveling time $t_f - t_0$. This method minimizes the consumption energy between t_0 and t_f by optimizing the velocity profile. Therefore, the objective function and the constraint conditions are expressed as

$$\text{min.} \quad W_{\mathrm{in}} = \int_{t_0}^{t_f} P_{\mathrm{in}}(\boldsymbol{x}(t), \boldsymbol{u}(t))dt, \tag{33}$$

$$\text{s.t.} \quad \dot{\boldsymbol{x}} = \boldsymbol{f}(\boldsymbol{x}(t), \boldsymbol{u}(t)) = \begin{bmatrix} \frac{1}{M}\left[F_{\mathrm{all}} - \mathrm{sgn}(V)(F_{\mathrm{DR}}(V) + F_{\mathrm{CR}}(V, R))\right] \\ V(t) \\ -\frac{2(C_f + C_r)}{MV}\beta - \left[\frac{2(l_f C_f - l_r C_r)}{MV^2} - 1\right]\gamma + \frac{2C_f}{MV}\delta_f \\ -\frac{2(l_f C_f + l_r C_r)}{I}\beta - \frac{2({l_f}^2 C_f + {l_r}^2 C_r)}{IV}\gamma + \frac{2 l_f C_f}{I}\delta_f \end{bmatrix}, \tag{34}$$

$$\chi(\boldsymbol{x}(t_0)) = \boldsymbol{x}(t_0) - \boldsymbol{x_0} = \begin{bmatrix} V(t_0) - V_0 \\ X(t_0) - X_0 \\ \beta(t_0) - \beta_0 \\ \gamma(t_0) - \gamma_0 \end{bmatrix} = \boldsymbol{0}, \tag{35}$$

$$\psi(\boldsymbol{x}(t_f)) = \boldsymbol{x}(t_f) - \boldsymbol{x_f} = \begin{bmatrix} V(t_f) - V_f \\ X(t_f) - X_f \\ \beta(t_f) - \beta_f \\ \gamma(t_f) - \gamma_f \end{bmatrix} = \boldsymbol{0}, \tag{36}$$

where W_{in} is the consumption energy, $\boldsymbol{x}$ is the state variable, $\boldsymbol{u}$ is the control variable, $\boldsymbol{x_0}$ is the initial condition, and $\boldsymbol{x_f}$ is the terminal condition.

$$\boldsymbol{x}(t) = \begin{bmatrix} V(t) \\ X(t) \\ \beta(t) \\ \gamma(t) \end{bmatrix}, \boldsymbol{u}(t) = \begin{bmatrix} F_{all}(t) \\ \delta_f(t) \end{bmatrix}. \tag{37}$$

The optimal velocity profile can be calculated by solving this optimal control problem numerically. In this paper, the front steering angle is given by (15) in optimization by assuming that the vehicle is brought into stationary circular turn and runs along the designated course.

4 Simulations

Simulations were conducted to verify the effectiveness of the proposed method. In this paper, three velocity profile generation methods are compared.

4.1 Comparison Conditions

In this paper, the vehicle velocity profile is optimized on the assumption that the vehicle runs along the course shown in Fig. 7. The following three cases are considered, and the traveling time $t_f - t_0$ of each case is 35.0 s.
Conventional 1: The conventional method 1 optimizes a_x of (38) to minimize the consumption energy in consideration of cornering.

$$V(t) = \begin{cases} V_0 + a_x t & (t_0 < t < t_1) \\ V_{\max} & (t_1 < t < t_2) \\ V_{\max} - a_x t & (t_2 < t < t_f) \end{cases}, \tag{38}$$

where

$$t_1 = \frac{V_{\max} - V_0}{a_x} + t_0, \tag{39}$$

$$t_2 = t_f - \frac{V_{\max} - V_f}{a_x}. \tag{40}$$

Conventional 2: The conventional method 2 optimizes a_x of (38) to minimize the consumption energy in consideration of cornering.

$$V(t) = \begin{cases} V_0 + a_x t & (t_0 < t < t_1) \\ V_{\max} & (t_1 < t < t_2) \\ V_{\max} - \frac{1}{M}\int_{t_2}^{t_3} (F_{\text{DR}}(V) + F_{\text{CR}}(V,R))dt & (t_2 < t < t_3) \\ V(2t_3 - t) & (t_3 < t < t_f) \end{cases}, \tag{41}$$

where

$$t_1 = \frac{V_{\max} - V_0}{a_x} + t_0, \tag{42}$$

$$t_2 = t_1 + \frac{1}{V_{\max}}\left(L - \frac{{V_{\max}}^2 - {V_0}^2}{2a_x}\right), \tag{43}$$

$$t_3 = \frac{t_f + t_0}{2}. \tag{44}$$

Proposed The velocity profile is optimized to minimize the consumption energy by solving the optimal control problem shown in section 3.

4.2 Loss Separation

To analyze which loss has great effect on optimizing velocity profile, $P_{\rm out}$ is separated as: the power stored as the kinetic energy of the vehicle mass $P_{\rm M}$, the sum of the power stored as the rotational energy of each wheel $P_{\rm J}$, the loss caused by the driving resistance $P_{\rm DR}$, the loss caused by the cornering resistance $P_{\rm CR}$, and the sum of the losses caused by the slip of each wheel $P_{\rm S}$:

$$P_{\rm out} = P_{\rm M} + P_{\rm J} + P_{\rm DR} + P_{\rm CR} + P_{\rm S}, \tag{45}$$

$$P_{\rm M} = \frac{d}{dt}\left(\frac{1}{2}MV^2\right), \tag{46}$$

$$P_{\rm J} = 2\sum_{j=f,r}\frac{d}{dt}\left(\frac{1}{2}J_{\omega_j}{\omega_j}^2\right), \tag{47}$$

$$P_{\rm DR} = F_{DR}(V)V, \tag{48}$$

$$P_{\rm CR} = F_{CR}(V,R)V, \tag{49}$$

$$P_{\rm S} = F_{\rm all}V\sum_{j=f,r}\frac{1}{2}\lambda_j. \tag{50}$$

The integrated values of these values are described as

$$W_X = \int_{t_0}^{t_f} P_X(\boldsymbol{x}(t),\boldsymbol{u}(t))dt, \tag{51}$$

where the subscript X represents “out”, “M”, “J”, “DR”, “CR”, “S”, “c”, and “i”. $W_{\rm M}$ and $W_{\rm J}$ can be recovered during decelerating, and they are equal zero in all cases if $V_0 = V_{\rm f}$.

4.3 Control System Design

Fig. 8 shows the velocity control system. The input is the vehicle velocity reference V^*, and these controllers generate the total driving-braking force reference $F^*_{\rm all}$. And then, $F^*_{\rm all}$is distributed to the front and rear driving-braking force reference F^*_j. Considering the slip ratio, the front and rear torque reference T^*_j is given as

$$T^*_j = rF^*_j + \frac{J_{\omega_j}a^*_x}{r}(1+\lambda^*_j), \tag{52}$$

where the second term of the right hand side means the compensation of the inertia of the wheels. In this paper, λ^*_j is given as

$$\lambda^*_j = \begin{cases} 0.05 & (a^*_x > 0) \\ 0 & (a^*_x = 0) \\ -0.05 & (a^*_x < 0) \end{cases}. \tag{53}$$

The vehicle velocity controller $C_{\rm PI}$ is a PI controller, and it is designed by the pole placement method. The plant of the vehicle velocity controller is expressed as

$$\frac{V}{F_{\rm all}} = \frac{1}{Ms}. \tag{54}$$

In the experiments, the poles of the vehicle velocity controller are set to -5 rad/s.

4.4 Simulation Results

Figs. 9 shows the simulation results. The vehicle velocity of conventional method 2 during cornering is lower than that of conventional method 1. Therefore the loss caused by the cornering resistance is reduced by 13.2 % compared with conventional method 2 as shown in Fig. 9(d) because the cornering resistance is proportional to biquadratic of the vehicle velocity. Compared with conventional method 1, conventional method 2 reduces 1.45 % of the consumption energy.

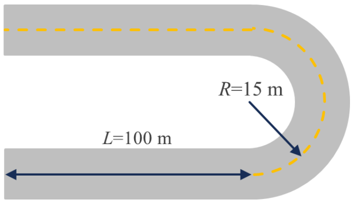

Figure 7: Driving course.

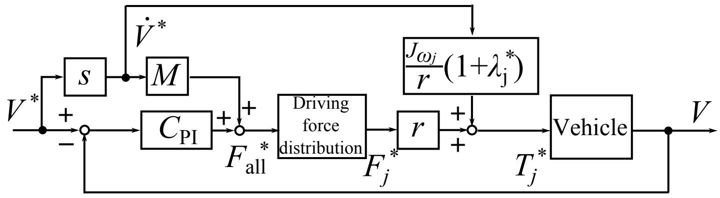

Figure 8: Vehicle speed control system.

Proposed method first accelerates higher speed than conventional methods, then decelerates before the corner, and finally accelerates around the end of the corner. The loss caused by the cornering resistance is reduced by 49.0 % compared with conventional method 1 as shown in Fig. 9(d) because the vehicle velocity during cornering is lower than both conventional methods. If the velocity during cornering is lower than proposed method, the loss caused by the cornering resistance becomes smaller whereas the copper loss and the loss caused by the driving resistance become larger because maximum speed and acceleration must become larger. The increase rate of the copper loss is only 1.53 % because time driving with large driving force is relatively short whereas the maximum acceleration is 51.0 % larger than conventional method 1. The increase rate of the loss caused by the driving resistance is only 0.57 % because the vehicle velocity during cornering is smaller than conventional method whereas the maximum speed is 16.1 % larger than conventional method 1. Compared with conventional method 1, proposed method 2 reduces 5.63 % of the consumption energy.

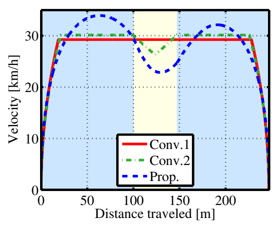

(a) Velocity V.

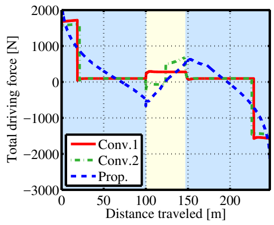

(b) Total driving force F_{all}.

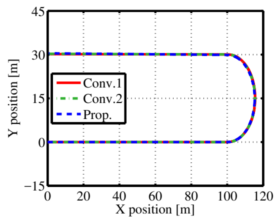

(c) XY position.

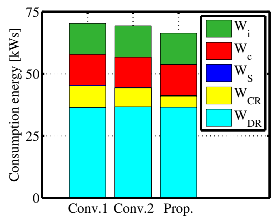

(d) Consumption energy W_{in}.

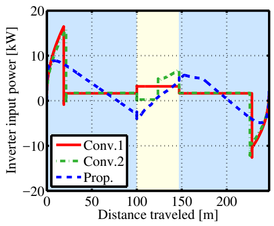

(e) Inverter input power P_{in}.

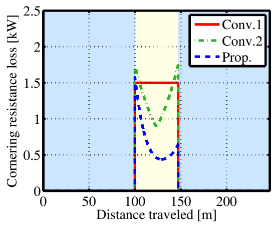

(f) Cornering resistance loss P_{CR}.

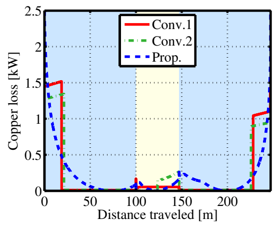

(g) Copper loss P_{c}.

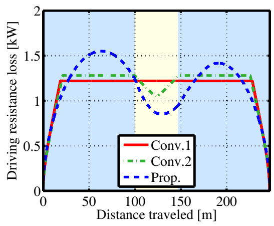

(h) Driving resistance loss P_{DR}.

Figure 9: Simulation results (Corner).

5 Experiment

Experiments were conducted to verify the effectiveness of the proposed method. In the experiments, the vehicle velocity is controlled by the velocity control system shown in Fig. 8, and the front steering angle is controlled by hand to track the designated course.

5.1 Experimental Results

Experiments were conducted five times under respective conditions, using the same conditions as simulations. In the experiments, we assumed that the vehicle velocity V is the average of all the wheel velocities. The inverter input power P_{in} was calculated as

$$P_{\mathrm{in}} = V_{\mathrm{dc}} \sum_{j=f,r} I_{\mathrm{dc}j}, \tag{55}$$

where V_{dc} is the measured input voltage of the inverter and $I_{\mathrm{dc}j}$ is the measured input current of the front and rear inverters. P_{in} includes inverter loss.
Fig. 10 shows the experimental results. According to Fig. 10(b), the total driving force shows the same tendency as simulation results. It means that modeling of the driving resistance and the cornering resistance is valid. According to Fig. 10(c), the inverter input power shows the same tendency as simulation results. Compared with conventional method 1, conventional method 2 reduces 1.58 % of the consumption energy and proposed method does 2.33 % of that. Decrease rate of consumption energy is smaller than simulations because the inverter input power includes modeling error.

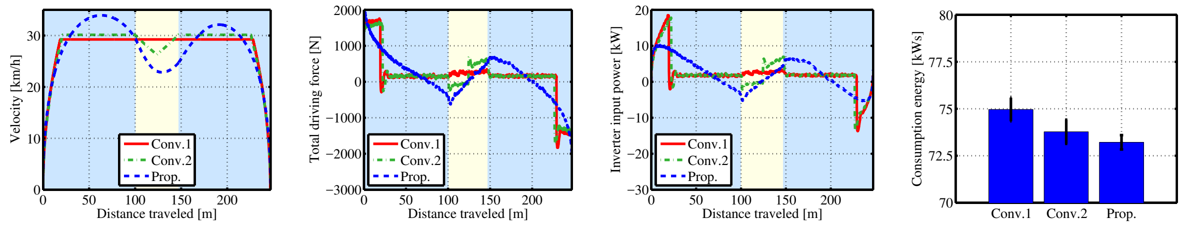

(a) Velocity V.

(b) Total driving force F_{all}.

(c) Inverter input power P_{in}.

(d) Consumption energy W_{in}.

Figure 10: Experimental results (Corner).

6 Conclusion

In this paper, READ system is extended to be applied to curvy road. The cornering resistance is modeled as a function which is proportional to biquadratic of the vehicle velocity on the assumption that the vehicle is brought into stationary circular turn. Proposed READ system can generate the optimal velocity profile by solving the optimal control problem numerically. Optimal velocity profile is mainly decided by trade off among the loss caused by the cornering resistance, the driving resistance, and the copper loss. In the experimental results, proposed method reduces 2.33 % of the consumption energy compared with conventional method 1.
In this paper, the torques of the right and left motors are equal. Therefore future work is to introduce velocity profile considering moments by differential torque of right and left motors.

Acknowledgment

This research was partly supported by Industrial Technology Research Grant Program from New Energy and Industrial Technology Development Organization (NEDO) of Japan (number 05A48701d), the Ministry of Education, Culture, Sports, Science and Technology grant (number 22246057 and 26249061), and the Core Research for Evolutional Science and Technology, Japan Science and Technology Agency (JST-CREST). This result is a part of work in the project team of JST-CREST named “Integrated Design of Local EMSs and their Aggregation Scenario Considering Energy Consumption Behaviors and Cooperative Use of Decentralized In-Vehicle Batteries.”

References

[1] Y. Hori, *Future vehicle driven by electricity and control - research on four-wheel-motored “UOT Electric March II”*, IEEE Trans. on Industrial Electronics, ISSN 0278-0046, 51(2004), 954-962.

[2] D. Sato and J. Itoh, *Loss Minimization Design Using Permeance Method for Interior Permanent Magnet Synchronous Motor*, IEEJ Trans. on Industry Applications, ISSN 0913-6339, 135(2014), pp. 138-146 (in Japanese).

[3] Y. Hosoyamada et.al., *High Efficiency Series Chopper Power Train for Electric Vehicles Using a Motor Test Bench*, IEEJ Journal of Industry Applications, ISSN 2187-1094, 4(2015), pp. 460-468.

[4] J. Shin et.al., *Design and Implementation of Shaped Magnetic-Resonance-Based Wireless Power Transfer System for Roadway-Powered Moving Electric Vehicles*, IEEE Trans. on Industrial Electronics, ISSN 0278-0046, 61(2014), pp. 1179-1192.

[5] J. Zhang et.al., *Data-Driven Intelligent Transportation Systems:A Survey*, IEEE Trans. on Intelligent Transportation Systems, ISSN 1524-9050, 12(2011), pp.1624-1639.

[6] J. W. Kwon and D. Ghwa, *Adaptive Bidirectional Platoon Control Using a Coupled Sliding Mode Control Method*, IEEE Trans. on Intelligent Transport Systems, ISSN 1524-9050, 15(2014), pp.2040-2048.

[7] M. Ferreira and P. M. d'Orey, *On the Impact of Virtual Traffic Lights on Carbon Emissions Mitigation*, IEEE Trans. on Intelligent Transport Systems, ISSN 1524-9050, 13(2002), pp. 284-295.

[8] Y. Ikezawa, H. Fujimoto, and Y. Hori, *Range Extension Autonomous Driving for Electric Vehicles Based on Optimal Velocity Trajectory Generation and Front-Rear Driving-Braking Force Distribution*, IEEJ Journal of Industry Applications, ISSN 2187-1094, 5(2016), pp. X-X.

[9] H. Yoshida and H. Fujimoto, *Range Extension Autonomous Driving for Electric Vehicles Based on an Optimal Vehicle Velocity Trajectory Considering Road Gradient Information*, The 1st IEEJ International Workshop on Sensing, Actuation, and Motion Control (2015), pp. N/A.

[10] H. B. Pacejka and E. Bakker, *The Magic Formula Tyre Model*, Vehicle System Dynamics: International Journal of Vehicle Mechanics and Mobility, ISSN 1744-5159, 21(1992), pp. 1-18.

[11] H. Fujimoto and S. Harada, *Model-Based Range Extension Control System for Electric Vehicles With Front and Rear Driving-Braking Force Distributions*, IEEE Trans. on Industrial Electronics, ISSN 0278-0046, 62(2015), pp.3245-3254.

[12] S. Morimoto et.al., *Loss Minimization Control of Permanent Magnet Synchronous Motor Drives*, IEEE Trans. on Industrial Electronics, ISSN 0278-0046, 41(1994), pp. 511-517.

Authors

Mr. Yuta Ikezawa received the B.S. degree in Department of Electrical and Electronic Engineering from The University of Tokyo, Tokyo, Japan, in 2015. He is currently working towards the M.S. degree in the Department of Advanced Energy, The University of Tokyo, Chiba, Japan. His research interests are optimal control systems for electric vehicle. Mr. Ikezawa is a student member of IEEE, IEEJ and SAE-Japan.

Dr. Hiroshi Fujimoto received the Ph.D. degree in the Department of Electrical Engineering from the University of Tokyo in 2001. In 2001, he joined the Department of Electrical Engineering, Nagaoka University of Technology, Niigata, Japan, as a research associate. From 2002 to 2003, he was a visiting scholar in the School of Mechanical Engineering, Purdue University, U.S.A. In 2004, he joined the Department of Electrical and Computer Engineering, Yokohama National University, Yokohama, Japan, as a lecturer and he became an associate professor in 2005. He is currently an associate professor of the University of Tokyo since 2010. He received the Best Paper Award from the IEEE Transactions on Industrial Electronics in 2001 and 2013, Isao Takahashi Power Electronics Award in 2010, and Best Author Prize of SICE in 2010. His interests are in control engineering, motion control, nano-scale servo systems, electric vehicle control, and motor drive. Dr. Fujimoto is a member of IEEE, the Society of Instrument and Control Engineers, the Robotics Society of Japan, and the Society of Automotive Engineers of Japan.

Dr. Daisuke Kawano received Doctoral degree in the Department of Mechanical Engineering from Doshisha University, Japan in 2003. Since February 2003, he has been affiliated with National Traffic Safety and Environment Laboratory, Japan. He works on environmental performance of next-generation vehicles and alternative fuels.

Dr. Yuichi Goto received B.S. and M.S. degrees in the Department of Science from Kyoto University, Japan in 1977 and 1979, respectively. He received Ph.D in the Department of Mechanical Engineering from Hokkaido University, Japan in 2002. From 1979 until 2001, he has been affiliated with Traffic Safety and Nuisance Research Institute (TSNRI) in Ministry of Transport, Japan. From 2001 until now, he has been affiliated with National Traffic Safety and Environment Laboratory (NTSEL) in Ministry of Land, Infrastructure, Transport and Tourism, Japan. He works as a research coordinator of NTSEL.

Ms. Misaki Tsuchimoto received a bachelor's degree in Department of engineering and design from Shibaura Institute of Technology, Japan in 2014. Since April 2014, she has been with ONO SOKKI CO., Ltd. She works on the design of a motion control of automotive-testing systems.

Mr. Koji Sato received B.E. and M.E. degrees in Department of mechanical and control engineering from The University of Electro-Communications, Japan in 1992 and 1994, respectively. Since April 1994, he has been with ONO SOKKI CO., Ltd. He works on the design of a motion control of automotive-testing systems.